New multi-standard dual-wideband and quad-wideband asymmetric step impedance resonator filters with wide stop band restriction

Author's draft of the accepted paper for International Journal of RF and Microwave Computer-Aided Eng., April 2019

New Multi-standard Dual-Wideband and Quad-Wideband Asymmetric Step Impedance Resonator Filters with Wide Stop Band Restriction

Yasir I. A. Al-Yasir, Yuxiang Tu, Naser Ojaroudi Parchin, Ahmed M. Abdulkhaleq, Jamal Kosha, Atta Ullah, Raed A. Abd-Alhameed, James M. Noras

Abstract —**New multi-standard wide band filters with compact sizes are designed for wireless communication devices. The proposed structures realize dual-wideband and quad-wideband characteristics by using a new skew-symmetrical coupled pair of asymmetric stepped impedance resonators, combined with other structures. The first and second dual-wideband filters realize fractional bandwidths (FBW) of 43.2%/31.9% at the central frequencies (CF) of 1.875/1.63 GHz, and second bandwidths of 580 MHz/1.75 GHz at CF of 5.52/4.46 GHz, respectively. The proposed quad-band filter realizes its first/second/third/fourth pass bands at CF 2.13/5.25/7.685/9.31 GHz with FBW of 46.0%/11.4%/4.6% and 5.4%, respectively. The wide pass bands are attributed to the mutual coupling of the modified ASIR resonators and their bandwidths are controllable by tuning relative parameters while the wide stop band performance is optimized by the novel interdigital cross coupled line structure and parallel uncoupled microstrip line structure. Moreover, the quad band is generated by introducing the novel defected rectangle structure. These multi-standard filters are simulated, fabricated and measured, and measured results agree well with both simulated results and theory predictions. The good in-band and out-of-band performances, the miniaturized sizes and simple structures of the proposed filters make them very promising for applications in future multi-standard wireless communication.**

Index Terms —**Asymmetrical stepped-impedance Resonator (ASIR), dual-wide band, quad-wide band bandpass filter (BPF), multi-standard, wide stopband.**

I. INTRODUCTION

Ever-increasing demand for compact wireless transceivers continues to impact the field of microwave and radio frequency communication [1] [2]. One of the most important modules in such systems is the filter [3]-[22], and its performance dominates the whole wireless communication system.

Compared to the traditional stepped impedance resonator (SIR) with two step discontinuities, the asymmetric SIR has only one discontinuity but retains the characteristic of controllable spurious modes.

Y. I. A. Al-Yasir, Y. Tu, N. Ojaroudi Parchin, Ahmed M. Abdulkhaleq, J. Kosha, A. Ullah, R. A. Abd-Alhameed, J. M. Noras are with Radio Frequency, Communication and Network research group, School of Electrical Engineering and Computer Science, Bradford University, Bradford, West Yorkshire, BD7 1DP, UK (email: R.A.A.Abd@bradford.ac.uk)

It has advantages of compact size, less loss, and versatility in design, particularly for high-order BPFs such as dual band, triple band and quad band BPFs because of its inherently higher order resonant modes. It has recently been used to construct high-performance BPFs [3]-[7], and in [6] and [7], two-stage wide-stopband BPFs using asymmetric SIRs have been proposed. The schemes of distributing spurious resonant frequencies of asymmetric SIR with wide stop band performance are realized. Additionally, with fewer discontinuities, the asymmetric SIR can be easily folded and coupled, and this results in a lower insertion loss and greater size reduction.

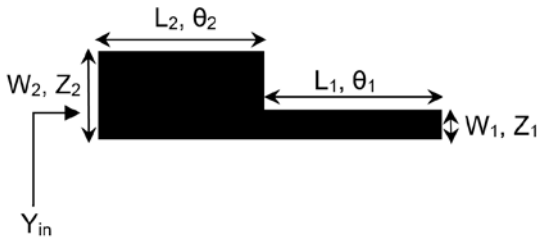

Fig. 1. Structure of an asymmetric SIR [4].

On the other hand, with the current increasingly stringent limitations on frequency spectrum resources and the development of advanced multi-standard wireless communication systems, multi-standard internal filters have become a necessity for state-of-the-art multifunction "smart phones" and wireless transceivers for mobile devices. Such filters are generally required to be capable of covering the frequency bands of the Global Positioning System (GPS: band centered at 1.57 GHz), the Global System for Mobile Communication (GSM: 1800/1900 MHz etc.) and the Universal Mobile Telecommunications System (UMTS: 1710-1880/1850-1990/1920-2170 MHz etc.). Moreover the ever expanding implementation of the Wireless Local Area Network (WLAN) adds the requirement of a band centered at 2.4 GHz and/or 5.2 GHz. Many dual band filters have recently been designed to satisfy such demanding requirements. However, many of these that are also miniaturized fail to fully cover all the required bands, especially at the lower frequencies due to the narrower dual bandwidth [3][4][5][9][16], or their size or thickness makes them difficult to integrate within mobile devices or portable wireless modules [7][12][13][15].

In this paper, we propose novel multi-standard asymmetric SIR filters including both dual-wideband filters with wide stopbands and a quad-wideband filter. These filters are capable of generating two and four wide operating bands that effectively cover the GPS/GSM/UMTS/IEEE802.11a application in mobile devices, including GPS(1.75 GHZ), GSM1800 (1710-1880 MHz), GSM1900 (1850–1990 MHz), UMTS (1920–2170 MHz) and IEEE 802.11a (5 GHz) bands. Meanwhile, in-band and out-of-band performance of the proposed filters is further enhanced by novel structures. To the best of authors' knowledge, these structures realize for the first time dual wideband and wide stop band resulting from the restriction of high order harmonic frequencies at the same time in dual wideband [8][10][11][13]-[15] and asymmetric SIR filters [3]-[7]. Moreover, the proposed structures use the capacitive coupling of only two miniaturized resonators to realize dual-wideband and quad-wideband responses without such extra structures such as via holes or defected ground planes, and so are unique among dual-wideband and quad-wideband filters [10]-[13][15]. The filters are simulated and optimized using CST microwave studio software [23].

II. RESONANCE CHARACTERISTICS OF THE ASYMMETRIC SIR UNIT AND THE SKEW-SYMMETRICAL ASYMMETRIC SIR COUPLED PAIR

A. Characteristic of the Asymmetric SIR Unit

The asymmetric SIR shown in Fig.1, adopted from [4], consists of sections with low and high characteristic impedances Z_1 and Z_2. The physical lengths L_1 and L_2, physical widths W_1 and W_2, and electrical lengths θ_1 and θ_2 are shown for the two sections with Z_1 and Z_2, respectively. The characteristic impedance ratio K and the length ratio α are defined as follows:

$$K = \frac{Z_2}{Z_1} \tag{1}$$

$$\alpha = \frac{\theta_2}{\theta_1 + \theta_2} \tag{2}$$

where α is located in the range of (0, 1).

The input admittance Y_{in} of the proposed asymmetric SIR unit is derived as:

$$Y_{in} = \frac{j}{Z_2}\frac{K\tan\theta_1 + \tan\theta_2}{1 - K\tan\theta_1\tan\theta_2} \tag{3}$$

It is known that resonance of the proposed asymmetric SIR occurs when $Y_{in} = 0$. Based on (3), this resonance happens when

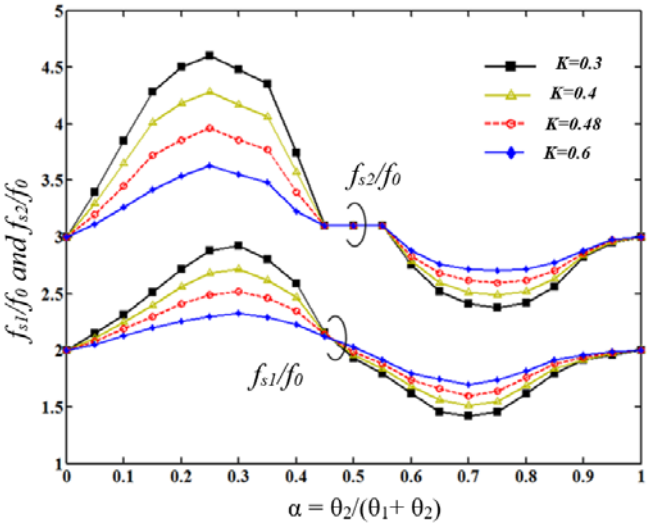

Fig. 2. f_{s1} (the first spurious frequency) and f_{s2} (the second spurious frequency) normalized by f_0 (the fundamental frequency) for the asymmetric SIR in Fig.1.

$$\frac{K\tan\theta_1 + \tan\theta_2}{1 - K\tan\theta_1\tan\theta_2} = 0 \tag{4}$$

From the solution of (4), the first and second spurious frequencies f_{s1} and f_{s2} are plotted in Fig.2, normalized by the fundamental frequency against α with different values of K. When α is more than 0.5, the normalized frequency f_{s1}/f_0 is greater than 2 and f_{s2}/f_0 is greater than 3, respectively. Also smaller K can result in greater normalized frequency when α is fixed. When α is greater than 0.5, the normalized frequency f_{s1}/f_0 is less than 2 and f_{s2}/f_0 is less than 3. Smaller K can result in lower normalized frequency for a fixed α.When K=1, f_{s1}/f_0 is equal to 2 and f_{s2}/f_0 is equal to 3. This means that in this limit a uniform impedance resonator is realized and the high order resonant frequency is an integer multiple of the fundamental frequency f_0. Therefore, the higher order spurious resonant modes, which depend on the choice of the characteristic impedance ratio K and the electric length ratio α, can be found by combining (2) and (4).

B. Characteristic of the Skew-Symmetrical Asymmetric SIR Coupled Pair

A skew-symmetrical asymmetric SIR coupled pair is illustrated in Fig.3. It contains two asymmetric SIR units connected through two high impedance coupled lines.

The coupling matrix referred to in [16] will not be discussed in this paper because of its non-wideband limitation [16][17]. The coupling between two ASIRs can be represented by a J-inverter susceptance $\overline{J_{1,2}}$ where the subscript 1 and 2 denotes the first and second passband. A larger value of $\overline{J_{1,2}}$ means a stronger coupling strength between two ASIRs. The normalized $\overline{J_{1,2}}$ can be determined by

$$\overline{J_{1,2}} = J_{1,2}Z_0 \tag{5}$$

where Z_0 represents the referred port impedance.

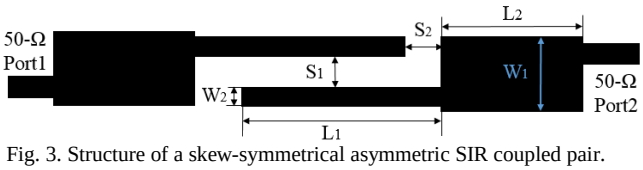

Fig. 3. Structure of a skew-symmetrical asymmetric SIR coupled pair.

The external quality factor $Q_{ex1,2}$ and the normalized J-inverter susceptance $\overline{J_{1,2}}$ can be related by [16]

$$Q_{ex1,2} = \frac{\pi}{2\overline{J_{1,2}}^2} \tag{6}$$

The external quality factor $Q_{ex1,2}$ can be further extracted by

$$Q_{ex1,2} = \frac{f_{c1,2}}{\Delta_{1,2}} = \frac{f_{c1,2}}{\Delta_{(\pm\frac{\pi}{2})1,2}} \tag{7}$$

where $f_{c1,2}$, $\Delta_{1,2}$, $\Delta_{(\pm\frac{\pi}{2})1,2}$, represents the central frequency, -3dB bandwidths, and the frequency bandwidth of phase curve changing $\left(\pm\frac{\pi}{2}\right)$ with respect to $f_{c1,2}$, respectively. $\overline{J_{1,2}}$ can be calculated by substituting the extracted $Q_{ex1,2}$ into equations (6) and (7).

From the full-wave EM simulation (CST software [23]), it is noted that the frequency response performance (in terms of bandwidth, return loss and insertion loss) is improved significantly at some frequency points in the SS-ASIR coupled pair while in other respects the performance is not changed much or degraded in comparison with the asymmetric SIR unit. Table I shows the frequency response transformation from asymmetric SIR unit to skew-symmetrical asymmetric SIR coupled pair. It can be seen that when the asymmetric SIR's electric length ratio α ranges from 0.4 to 0.5, the frequency response at frequency f_0, f_{s3} and f_{s4} enhances significantly in the SS-ASIR coupled structure, while it does not change much or degrades at f_{s1} and f_{s3}. When α=0.6, the frequency response at f_0, f_{s1} and f_{s3} enhances greatly, but it does not vary much or degrades at f_{s2} and f_{s4}. The transformation table is useful to analysis and transform frequency bands where the performance-enhanced frequency response appears into desired pass bands by considering the asymmetric SIR unit characteristic. It is also useful to analyse and transform frequency bands where the performance-degraded frequency response appears into stop bands or excite them to become pass band by modifying the SS-ASIR coupled structure.

C. The influence of electric length ratio α in SS-ASIRs

An inherent property of the skew-symmetrical asymmetric SIR (SS-ASIR) coupled pair is that the resonant frequency location and bandwidth performance are mainly influenced by the electric length ratio α when length L_1 is fixed, and is hardly affected by the impedance ratio K. This invariance characteristic is not found with the asymmetric SIR unit, where the normalized frequency (and resonant frequency) is closely related with K value. This characteristic of α=0.42 is shown in Fig.4: resonant frequency locations and their bandwidths are nearly fixed when α is fixed at 0.42, and these two parameters are little influenced by K. Similar phenomenon can be observed when α is fixed at other values. This means α is the main factor to influence the horizontal frequency response performance such as resonant frequency locations and bandwidths in SS-ASIR coupled structures.

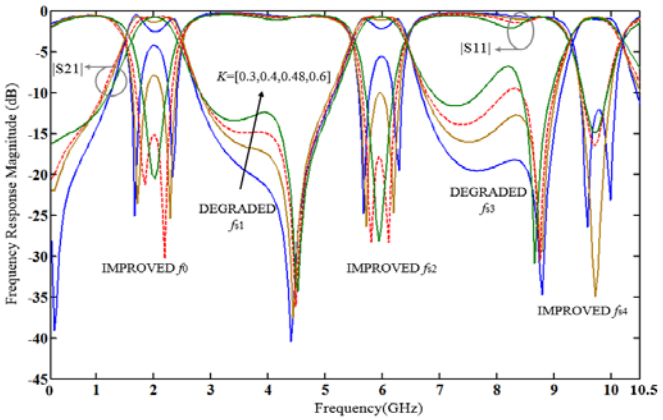

Fig. 4. Frequency characteristic curves of the SS-ASIR coupled pair when α=0.42, L1=11 mm and K=0.3, 0.4, 0.48 and 0.6.

D. The influence of impedance ratio K in SS-ASIRs

The return loss and insertion loss performance of enhanced f_0 and f_{s2} (seen in TABLE I. and Fig. 4) becomes better when K varies from 0.3 to 0.6. Meanwhile, the return loss and insertion loss performance of degraded f_{s1} and f_{s3} (seen in TABLE I and Fig. 4) become better and forms two spurious peaking finally. Similar phenomenon can be observed when K takes other values. Therefore, the impedance ratio K is a major influence on the vertical frequency response performance such as return loss and insertion loss in both pass-band and stop-band of SS-ASIR coupled structures. By considering the characteristic of SS-ASIR coupled pairs and of the asymmetric SIR unit, α=0.42 and K=0.48 are extracted to design the proposed filters. The performance-enhanced frequency bands at f_0 and f_{s2} are used to form the first and second pass band in the proposed dual-band and quad-band filters. The performance-degraded frequency band at f_{s3} and performance-enhanced frequency band at f_{s4} are unwanted in the proposed dual-band filters, but they are used to form the third and fourth pass band in the proposed quad-band filter.

Fig. 5 plots the variation of coupling bandwidth as a function of the gap size (S_1) between the two resonators. Increasing the gap between the resonators reduces the coupling bandwidth of the designed filer and vice versa. Given the required electrical length ratio α, coupling coefficients and external quality factor for the proposed filters, one may determine the proper specifications based on these factors.

TABLE I
THE TRANSFORMATION RELATIONSHIP OF IN-BAND PERFORMANCE OF SKEW-SYMMETRICAL ASYMMETRIC SIR COUPLED PAIR AND ASYMMETRIC SIR UNIT.
''IMPROVED'' MEANS SIGNIFICANT ENHANCEMENT OF PERFORMANCE AT RELATIVE FREQUENCY;
''NC/DE''MEANS NO SIGNIFICANT CHANGE OR DEGRADATION OF PERFORMANCE AT RELATIVE FREQUENCY POINT.WHEN α RANGES FROM 0.3 TO 0.7.

f / α	The Fundamental Frequency f_0	The First spurious Frequency f_{s1}	The Second spurious Frequency f_{s2}	The Third Spurious Frequency f_{s3}	The Fourth Spurious Frequency f_{s4}
0.3	NC/DE	Improved	NC/DE	Improved	NC/DE
0.4	Improved	NC/DE	Improved	NC/DE	Improved
0.42	Improved	NC/DE	Improved	NC/DE	Improved
0.5	Improved	NC/DE	Improved	NC/DE	Improved
0.55	Improved	NC/DE	NC/DE	Improved	NC/DE
0.6	Improved	Improved	NC/DE	Improved	NC/DE
0.65	Improved	Improved	NC/DE	NC/DE	Improved
0.7	Improved	Improved	NC/DE	NC/DE	NC/DE

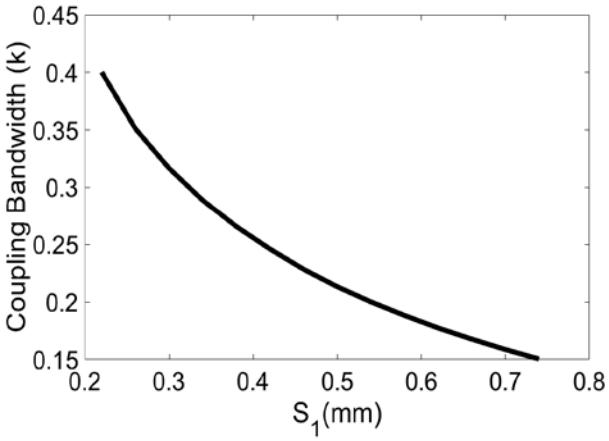

Fig. 5. Coupling bandwidth (K) with the gap size (S_1)

III. THE MODIFIED SKEW-SYMMETRICAL ASYMMETRIC SIR FILTER

A. SS-ASIR Filter with Open Stub and Folded Coupled Lines

In the skew-symmetrical asymmetric SIR filter, open stubs can be added to the low impedance lines, and the high impedance coupled lines can be folded, to achieve optimized performance. This geometry and its equivalent circuit are shown in Fig. 6 and Fig. 7, respectively. When two open stubs are moved from point A to C, the suppression performance of f_{s3} and f_{s4} becomes progressively better while the return loss performance of f_{s2} become worse from A to B and better from B to C. Meanwhile, the insertion loss and return loss performance of fundamental frequency f_o remains almost the same. Therefore, two open stubs are placed at point C. Fig. 8 shows the open stub effect on the frequency response of the SS-ASIR filter.

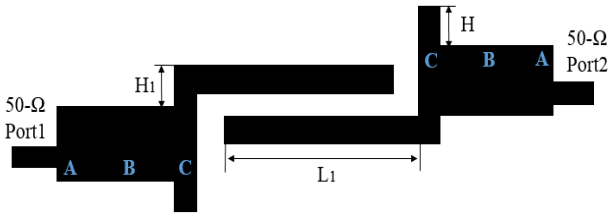

Fig. 6. Schematic diagram of an SS-ASIR filter with open stubs and folded coupled lines.

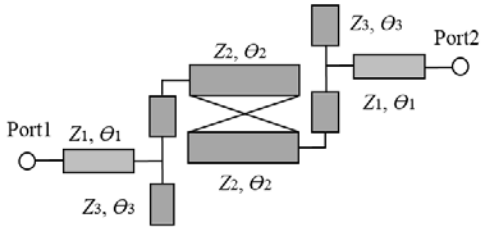

Fig. 7. The equivalent circuit of an SS-ASIR filter with open stubs and folded coupled lines.

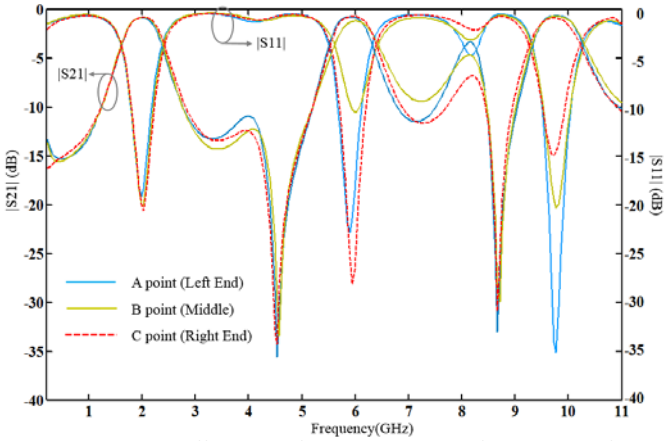

Fig. 8.The open stub effect on the frequency response of the SS-ASIR filter.

The high impedance lines are also folded to form the section of length H_1 between the high and low impedance lines. Compared to conventional coupled lines that are not folded, the suppression of unwanted transmission at frequency f_{s4} is greatly improved when the interval H1 varies from 0.5 mm to 0.9 mm. The change in the frequency response for this variation of H_1 is plotted in Fig. 9.

The design procedures for dual- and quint-wideband type BPFs can be summarized as follows:

1) Choose a suitable electrical length ratio α, thus setting the fundamental frequency f_0, and choose the characteristic impedance ratio K in the ASIR to improve insertion loss and return loss performance.

2) Analyze the transmission zero generating requirement of the interdigital cross-coupled line section added to the SS-ASIR structure and find suitable transmission zero locations.
3) According to previous results, tune the length of the interdigital cross-coupled line section to meet the required S_{21} to form a wide stop band for the dual-wideband type ASIR filter. The gap parameter S_5 is also tuned for optimized results.
4) Tune the length of the interdigital cross-coupled line section to enable a multi-band response with good isolation between operating bands.
5) The same design steps can be applied for the quint-wideband type BPF.

Because of the non-wideband limitation of the coupling matrix, coupling coefficients are not important in this design, while the external quality factor Q_{ex} can be discussed for performance optimization, as mentioned above.

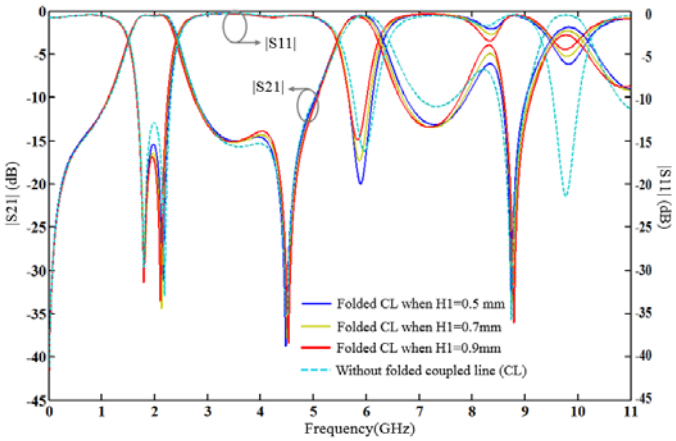

Fig. 9. The frequency response of the modified SS-ASIR filter versus frequency when H_1 varies from 0.5 mm to 0.9 mm.

B. The Modified SS-ASIR Filter with Interdigital Cross-Coupled Line (ICCL)

To further optimize the in-band and out-of-band performance of the proposed dual-band filter, auxiliary interdigital cross-coupled lines whose width and length are W_5 and L_5 are utilized to realize multi-path coupling between two modified ASIRs (MASIRs), as seen in Fig. 10. Compared to the single coupling route of A-C, at least two extra coupling routes including A-D and B-C are created by the inclusion of the auxiliary coupled lines. This interdigital multi-path coupling scheme of the modified SS-ASIR filter is shown in Fig. 10 (b). Moreover, because of the small distance between the main and auxiliary coupled lines, mutual coupling of A-B and C-D exists at the same time. This coupling is illustrated as dashed gray lines in Fig. 10 (b).

By including auxiliary coupled lines, the filter's out-of-band spurious frequency suppression performance and passband selectivity is considerably improved. The designed dual-band band pass filter (BPF) adopting an interdigital cross-coupled configuration produces a transmission zero (TZ) to approach f_{s3} and f_{s4}. The transmission zero occurs because of cancellation of the transmitted signals passing through different routes.

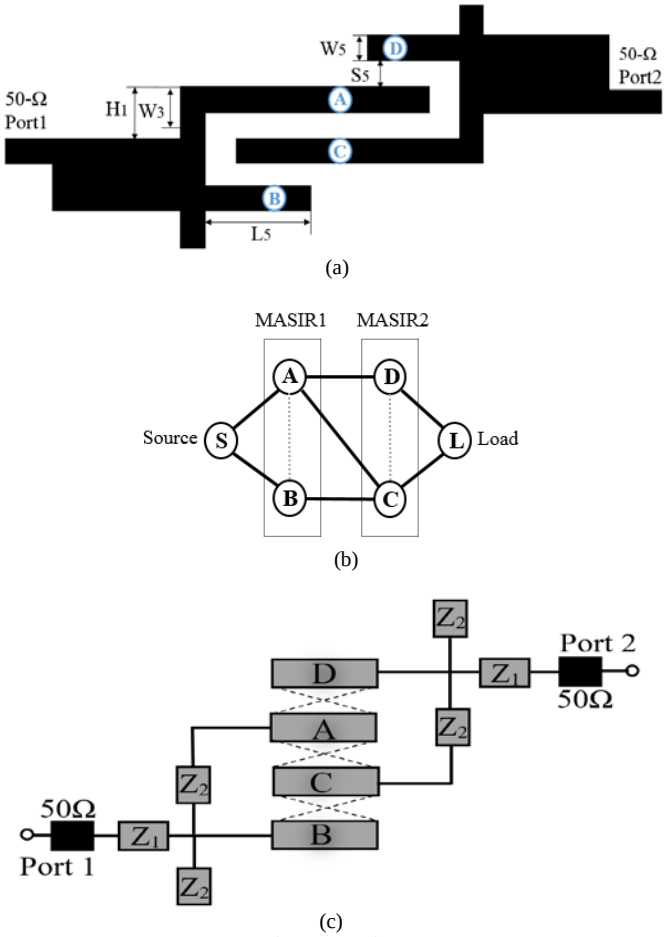

Fig. 10. Schematic diagram of the modified SS-ASIR coupled pair with interdigital cross coupled lines. (a) Structure. (b) Coupling routing scheme. A, B denotes the main coupling line and auxiliary cross coupling in MASIR1, respectively. C, D denotes the main coupling line and auxiliary cross coupling in MASIR2, respectively. (c) Equivalent circuit and coupling routing scheme for the SS-ASIRs with ICCLs.

As seen in Fig. 11, when the length of auxiliary coupled line L_5 ranges from 1.4-1.8 mm, optimized suppression of f_{s3} and f_{s4} is achieved. Also a wide stop band ranging from 6.3-12 GHz at the upper side of the second pass band is realized simultaneously. Also, the second pass band upper side's selectivity is improved with the two pass bands' return loss and insertion loss performance unaffected. Fig. 12 plots Q_{ex1}, Q_{ex2}, f_{s2}/f_0 and Q_{ex2}/Q_{ex1} versus S_5, which is the gap between auxiliary coupled line and main coupled line in the interdigital cross-coupled SS-ASIR filter. When S_5 changes from 0.1 mm to 0.8 mm, Q_{ex1} and f_{s2}/f_0 remain almost the same. This exhibits the stable invariance property of resonant frequency location in the SS-ASIR coupled structure and coincides with the frequency response in Fig. 4. Q_{ex2} decreases initially and increases a little later: this means that the bandwidth of f_{s2} can be controlled and expanded by tuning S_5. Therefore, S_5 is a factor that can tune Q_{ex2} and $\overline{J_{1,2}}$ in SS-ASIRs with the interdigital cross coupled line structure.

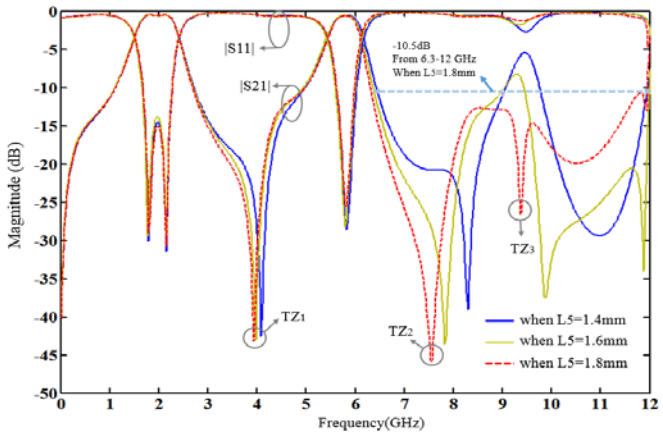

Fig. 11. The effect of L5 on the interdigital cross-coupled SS-ASIR.

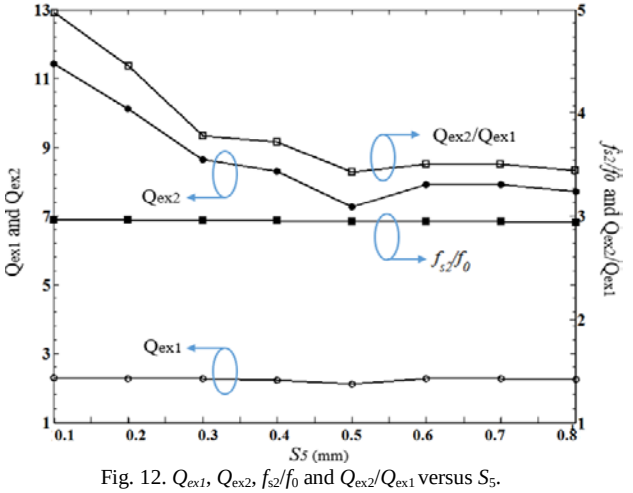

Fig. 12. Q_{ex1}, Q_{ex2}, f_{s2}/f_0 and Q_{ex2}/Q_{ex1} versus S_5.

The proposed filters were fabricated on an RO3010 substrate with a relative permittivity of 10.2, and measured using an HP8550 vector network analyser. The simulated *S*-parameters, measured *S*-parameters and photograph of the hardware realization of the designed dual-wideband SS-ASIRs with ICCLs are plotted in Fig. 13. Good agreement is observed between the simulated and measured results and the slight discrepancies are attributed to losses and fabrication errors. Dual wide bands are realized with good in-band return loss performance. The first pass band ranges from 1.47-2.28 GHz with central frequency of 1.875 GHz, bandwidth of 810 MHz and fractional band width (FBW) of 43.2%. It can be applied in the application of Global Positioning System (GPS: frequency band centered at 1.57 GHz), Global System for Mobile Communication (GSM: 1800/1900 MHz) and Universal Mobile Telecommunication System (UMTS: 1710-1880/1850-1990/1920-2170 MHz etc.). The second pass band ranges from 5.23-5.81 GHz with central frequency of 5.52 GHz, bandwidth of 580 MHz and fractional band width (FBW) of 10.5%. It can be applied in IEEE802.11a WLAN applications including 5G Wi-Fi. Moreover, good insolation is achieved between two pass bands, eliminating signal interference between dual-bands. The stop band ranges from 2.56-4.86 GHz with -10 dB suppression. Due to the adoption of the interdigital cross-coupled line structure, an extra transmission zero near f_{s3} and f_{s4} is created. A wide upper stop band ranging from 6.05-12.1 GHz with -10 dB suppression is generated, which can be seen in Fig. 13.

Parameters of the modified SS-ASIR filter and modified SS-ASIR filter with interdigital cross coupled lines (ICCLs) are shown in TABLE II.

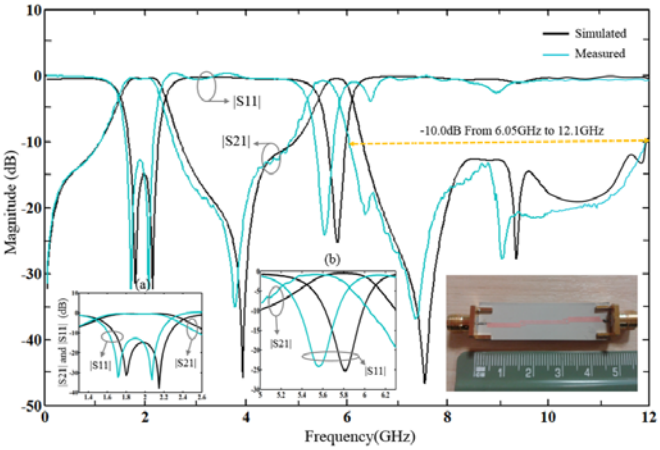

Fig. 13. Simulated, measured results and photograph of the hardware realization of an SS-ASIR with ICCLs. (a) Narrowband view of the first passband. (b) Narrowband view of the second passband.

TABLE II
PARAMETERS OF THE PROPOSED FOUR TYPES OF MODIFIED SS-ASIR FILTERS. ALL DIMENSIONS ARE IN MILLIMETERS.

Filter Type / parameter	The Modified SS-ASIR Filter	The Modified SS-ASIR Filter with ICCLs	The Modified SS-ASIR Filter with PUMLs	The Modified SS-ASIR Filter with DRS
L_1	11	11	11	11
L_2	15.6	15.6	15.6	15.6
W_1	1.6	1.6	1.6	1.6
W_3	0.4	0.4	0.4	0.4
L_5		1.81		
S_5		0.25		
W_5		0.42		
L_r			7.05	
L_m			2.32	
W_m			0.07	
Rd				0.6
W_d				4.65
H_d				1.2

C. The Modified SS-ASIR Filter with Parallel Uncoupled Microstrip Lines (PUMLs)

An uncoupled section located within conventional coupled lines is a useful method to achieve extra transmission zeros close to existing zeros created by the conventional coupled lines. Therefore, the results extending the stopband bandwidth with a better suppression level can be achieved. At the same time, this method can also give freedom to optimize the in-band performance of the original structure. Fig.14 shows the topological structure of the proposed modified SS-ASIR filter with parallel uncoupled microstrip lines. These parallel

uncoupled microstrip lines are formed by bending the original coupled lines outwards. The parallel uncoupled microstrip line's reference location to the original coupled line open end is Lr. The parallel uncoupled microstrip line height and inner gap is Lm and Wm, respectively.

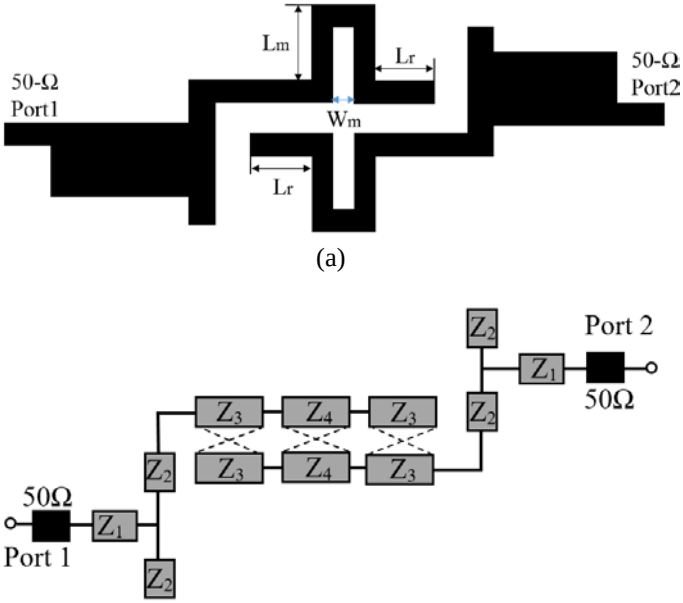

Fig. 14. (a) Schematic diagram of the proposed modified SS-ASIR filter with parallel uncoupled microstrip lines. (b) Equivalent circuit and coupling routing scheme for the SS-ASIR filter with PUMLs.

Compared to the former modified SS-ASIR filter with its interdigital cross-coupled line structure, the wider second pass band is achieved by adopting novel parallel uncoupled microstrip lines. In the former structure, Q_{ex1} and Q_{ex2} are equal to 2.28 and 9.37 when S_5=0.25 mm (as shown in Fig. 11), while $Q_{ex1,2}$ equal 2.71 and 3.48 when Lm=2.3 mm in this novel filter with PUMLs. This means $\overline{J_2}$ is improved greatly and a stronger coupling strength between two modified ASIRs is realized. Fig.15 shows the impact of the reference location parameter Lr on the frequency response of the filter with parallel uncoupled microstrip lines. It is noted that when Lr changes from 5.6 mm to 7 mm, the second pass band return loss performance is enhanced considerably and its bandwidth becomes wider resulting in forming a wide second pass band of more than 1.5 GHz. Meanwhile, the frequency response of the first pass band does not vary much. Hence, Lr is a vital factor to influence $\overline{J_2}$ and Q_{ex2}. Moreover, the parallel uncoupled microstrip line structure achieves one extra transmission zero nearby f_{s3} and f_{s4}, leading to an extended wide stopband bandwidth with better suppression level, as seen in Fig. 15.

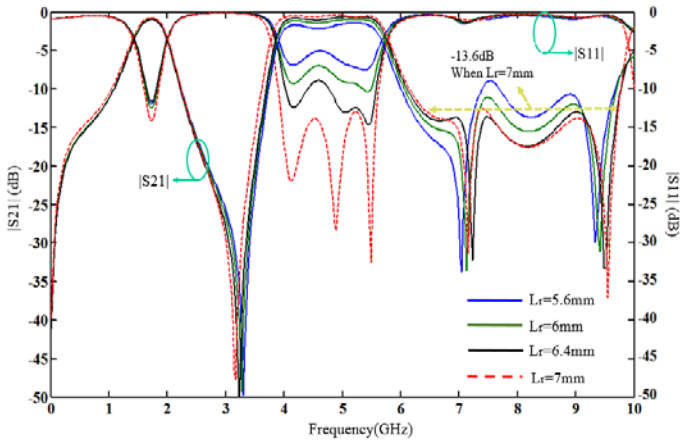

Fig. 15. Lr's impact on the frequency response of the SS-ASIR filter with PUMLs.

Fig.16 and Fig.17 show the impact of Lm on the frequency response of the SS-ASIR filter with PUMLs. In Fig.16, when Lm ranges from 0.5 mm to 5 mm, the fundamental frequency f_0 decreases continuously while Q_{ex1} increases slightly at first and increases dramatically when Lm is greater than 2.5 mm. This shows that the parallel uncoupled microstrip line height Lm can increase Qex1 and decrease $\overline{J_2}$ within a certain range. Fig. 17 plots the f_{s2}, Q_{ex2}, f_{s2}/f_0 and Q_{ex2}/Q_{ex1} versus against Lm. When Lm ranges from 0.5 mm to 1.5 mm, the rate of decline of Q_{ex2} is much faster than the rate of decline of f_{s2}, which means the bandwidth centred at f_{s2} is growing rapidly. When Lm ranges from 1.5 mm to 2.5 mm, the rate of decline of Q_{ex2} is almost the same as that of f_{s2}, that means that a wide band width centred at f_{s2} is formed and does not change much. When Lm ranges from 2.5 mm to 5 mm, Q_{ex2} increases as f_{s2} decreases, which means that the band centred at f_{s2} becomes narrower. In the whole process, f_{s2} moves from 5.6 GHz to 3.8 GHz with the second pass band being expanded to more than 1.5 GHz. Hence, Lm is also a factor to influence Q_{ex2} and strengthen $\overline{J_2}$.

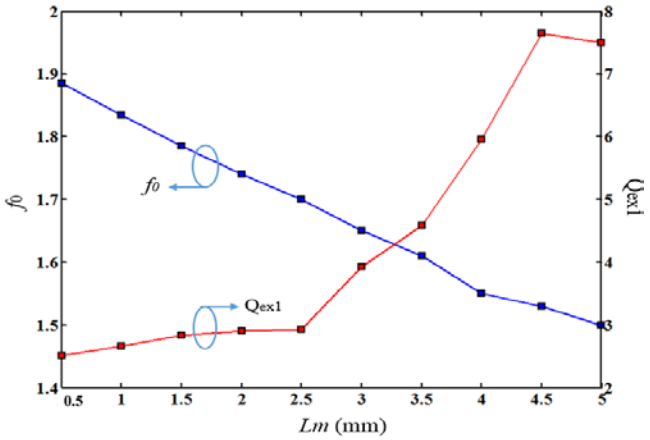

Fig. 16. f_0 and Q_{ex1} versus against Lm.

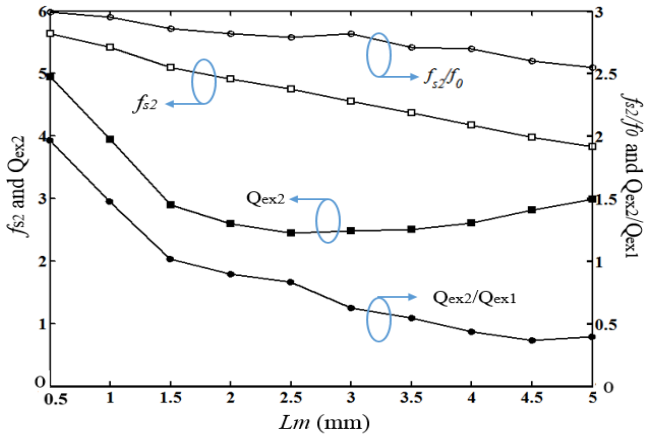

Fig. 17.f_{s2}, Q_{ex2}, f_{s2}/f_0 and Q_{ex2}/Q_{ex1} versus against Lm.

The reason for this can be explained by analysing the parallel uncoupled microstrip line unit, whose topological structure and frequency response are plotted in Fig. 18. As seen in the figure, the PUML unit forms a wide pass band of more than 1 GHz when Lm changes from 1 mm to 3 mm, and the pass band central frequency can be tuned by Lm. This result proves the advantage of the PUML structure to optimize the in-band performance of the filter. As for out-of-band performance, the PUML unit generates three transmission zeros (TZs) at both sides of the pass band, as plotted in Fig. 18. These three TZs can improve the isolation performance between two pass bands and the suppression level of undesired f_{s3} and f_{s4}.

The simulated *S*-parameters, measured *S*-parameters and photograph of the hardware realization of the designed dual-wideband SS-ASIRs with PUMLs are plotted in Fig. 19. There is good agreement between the simulated and measured results and the slight discrepancies are attributed to losses and fabrication errors. It can be seen that dual wide bands are realized with good in-band return loss performance. The first pass band ranges from 1.37-1.89 GHz with central frequency of 1.63 GHz, bandwidth of 520 MHz and fractional band width (FBW) of 31.9%. It can be applied in the application of Global Positioning System (GPS: frequency band centered at 1.57 GHz), Global System for Mobile Communication (GSM: 1800 MHz) and Universal Mobile Telecommunication System (UMTS: 1710-1880 MHz etc.). The second pass band ranges from 3.66-5.46 GHz with central frequency of 4.46 GHz, bandwidth of 1.8 GHz and fractional band width (FBW) of 33.0%. It can be applied in IEEE802.11a WLAN applications including 5G Wi-Fi. Moreover, good isolation is achieved between the two pass bands to eliminate signal interference between dual-bands. The stop band ranges from 2.12-3.5 GHz with -10 dB suppression. Due to the adoption of parallel uncoupled microstrip lines, an extra transmission zero near f_{s3} and f_{s4} is realized. A wide upper stop band ranging from 5.83-9.35GHz with -10dB suppression level is generated, which can be seen in Fig. 19.

The parameters of the modified SS-ASIR with parallel uncoupled microstrip lines are shown in TABLE II. A comparison of the performance of the modified SS-ASIR filter with ICCLs and PUMLs with previous work is shown in TABLE III.

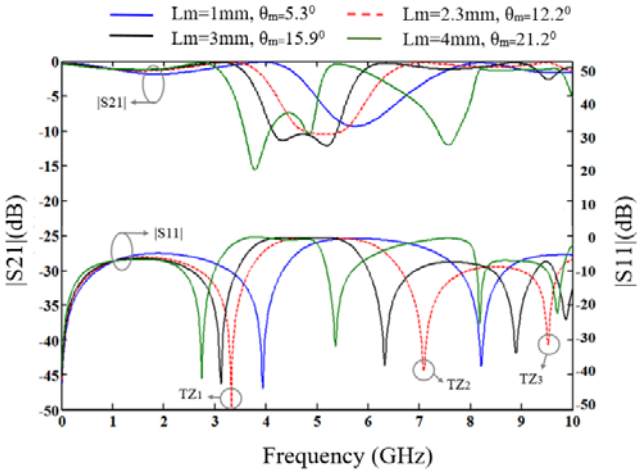

Fig. 18.The analysis of the PUML unit.

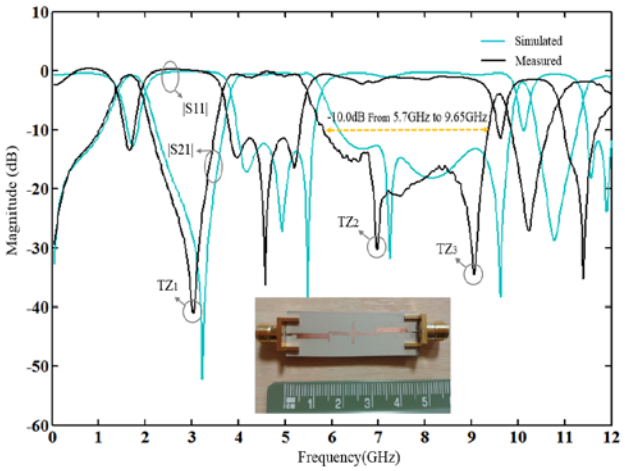

Fig. 19. Simulated, measured results and photograph of the hardware realization of an SS-ASIR with PUMLs.

D. The Modified SS-ASIR Filter with Defected Rectangular Structure (DRS)

The topological structure of the proposed modified skew-symmetrical asymmetric SIR Filter with defected structure is shown in Fig. 20. In contrast to the original skew-symmetrical asymmetric SIR filter, this filter has a defected rectangular structure (DRS) in each low impedance line, of width and length W_d and H_d, respectively. Its relative distance to the end of the feed line is Rd. By utilizing the defected rectangular structure, the performance-degraded frequency response at f_{s3} can enhance the frequency response and a new wide pass band can be excited centred at f_{s3}. The frequency response comparison between the modified SS-ASIR filter with and without DRS is plotted in Fig. 20 (c). By this means, a quad-band filter can be formed by adopting the defected rectangular structure in the SS-ASIR filter.

TABLE III
PERFORMANCE COMPARISION TO THE PROPOSED OF MODIFIED SS-ASIR FILTER WITH (A) ICCLS AND (B) PUMLS. ALL DIMENSIONS ARE IN MILLIMETERS.

Ref.	CF (GHz)	-3 dB FBW (%)	RL at CF(dB)	IL at CF(dB)	Size	No. of Transmission poles in each passband	Wide stop band Restriction
[8]	2.4/5.26	13.7/6.3	28/12	0.6/1.4	$0.46\lambda_g \times 0.42\lambda_g$	2/2	NO
[9]	2.43/3.73	4.5/6.1	24/24	2.5/1.3	$0.43\lambda_g \times 0.69\lambda_g$	1/1	NO
[15]	2.4/3.5	6.88/8.57	26/16	<0.3	$0.25\lambda_g \times 0.4\lambda_g$	2/2	NO
[19] Filter B	1.65/5.25	35.1/7.2	20/25	0.41/1.1	$0.33\lambda_g \times 0.03\lambda_g$	2/2	NO
This work (A)	1.875/5.52	43.2/10.5	12/25	0.39/0.87	$0.05\lambda_g \times 0.56\lambda_g$	1/3	YES
This work (B)	1.63/4.46	31.9/33.0	15/12	0.70/0.12	$0.09\lambda_g \times 0.56\lambda_g$	1/2	YES

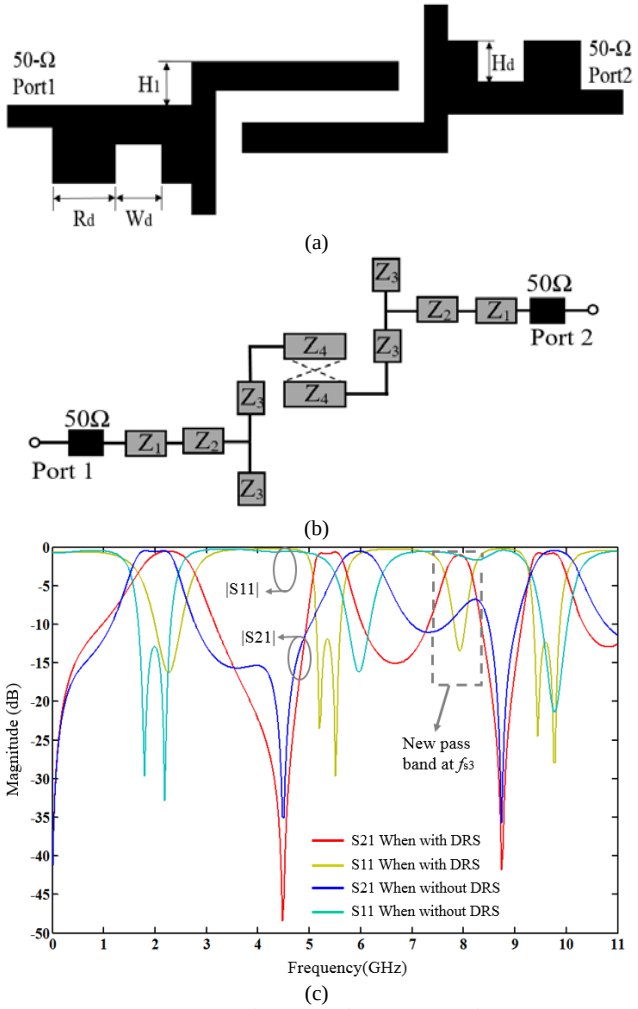

Fig. 20. Schematic diagram of the modified SS-ASIR filter with DRS: (a) structure. (b) Equivalent circuit and coupling routing scheme for the SS-ASIR filter with DRS. (c) The frequency response comparison of SS-ASIR filter with DRS and without DRS.

Fig. 21 plots the W_d's effect on SS-ASIR filter with DRS. In (a), when W_d varies from 2.5 to 6 mm, f_{s2}/f_0 decreases while Q_{ex1} remains almost the same: Q_{ex2} and Q_{ex2}/Q_{ex1} fluctuate in this process. This means f_{s2} does not follow the rules of invariance of resonant frequency location in the SS-ASIR coupled structure any more. In (b), Q_{ex3} varies from 12.1 to 26.8 and Q_{ex4} varies from 18.1 to 16 when W_d ranges from 2.5 to 6 mm, with Q_{ex3}/Q_{ex1} increasing continuously.

From EM simulations, it is noted that not all *f*s2, *f*s3 and *f*s4 in SS-ASIR coupled structures with DRS obey the rules of invariance of resonant frequency location: frequency shifting exists among all four pass bands compared to the situation that there is no DRS. This is because the basic structure of SS-ASIR coupled pairs is modified by the defected rectangular structure.

The simulated *S*-parameters, measured *S*-parameters and photograph of the hardware realization of the designed quad-wideband SS-ASIR filter with DMS are plotted in Fig. 22. There is good agreement between the simulated and measured results and the discrepancies are attributed to loss, fabrication errors and so on. It can be seen that dual wide bands are realized with good in-band return loss performance. The first pass band ranges from 1.64-2.62 GHz with central frequency of 2.13 GHz, bandwidth of 980 MHz and fractional band width (FBW) of 46.0%. It can be applied in the Global System for Mobile Communication (GSM: 1800 MHz/1900 MHz), Universal Mobile Telecommunication System (UMTS: 1710-1880/1850-1990/1920-2170 MHz etc.), ISM (Industrial, Scientific and Medical band: 2.4 GHz) and WLAN IEEE 802.11b/g/n applications including 2.4 GHz Wi-Fi. The second pass band ranges from 4.95-5.55GHz with central frequency of 5.25 GHz, bandwidth of 600MHz and fractional band width (FBW) of 11.4%. It can be used in IEEE802.11a WLAN applications. The third pass band ranges from 7.51-7.86GHz with central frequency of 7.685 GHz, bandwidth of 350MHz FBW of 4.6%, and can be used in electronic countermeasure (ECM) applications. The fourth pass band ranges from 9.06-

9.56GHz with central frequency of 9.31 GHz, bandwidth of 500MHz and FBW of 5.4%, suitable for X-band applications.

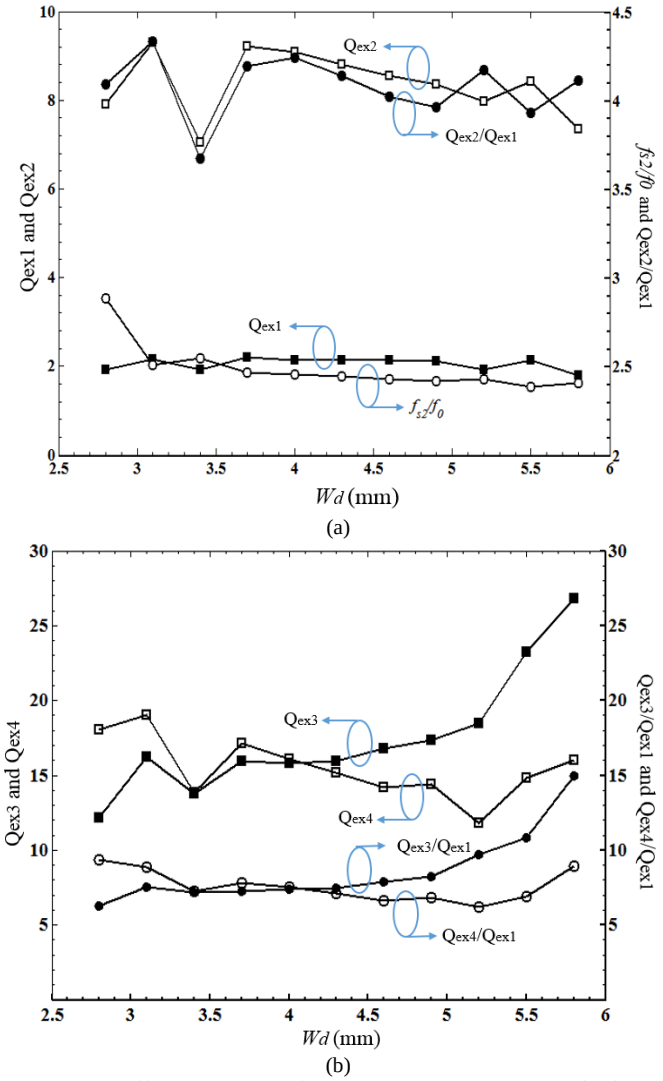

Fig. 21. Wd's effect on SS-ASIR filter with DRS. (a) Q_{ex1}, Q_{ex2}, $fs2/f_0$ and Q_{ex2}/Q_{ex1} versus against Wd. (b) Q_{ex3}, Q_{ex4}, Q_{ex3}/Q_{ex1} and Q_{ex4}/Q_{ex1} versus against Wd.

Moreover, good isolation is achieved between four pass bands, eliminating signal interference. The -10 dB suppression level stop bands range from 3.05-4.78GHz between the first and second pass band, 5.77-7.20 GHz between the second and third pass band, and 8.04-8.889 GHz between the third and fourth pass band. Moreover, two transmission zeroes located at 4.26 GHz and 8.46 GHz are formed to further enhance frequency selectivity, as shown in Fig.22. The parameters of modified SS-ASIR with DMS are shown in TABLE II. The size of the modified SS-ASIRs with DMS is $0.09\lambda_g \times 0.56\lambda_g$, where λ_g is the guide wavelength.

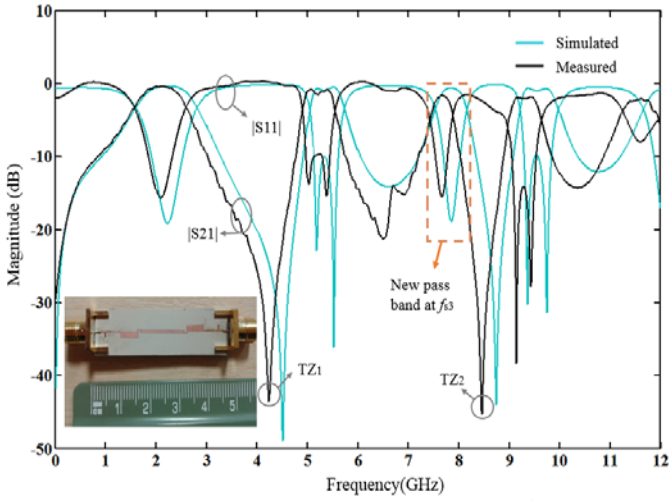

Fig. 22. Simulated, measured results and photograph of the hardware realization of the modified SS-ASIRs with DMS.

E. Surface Current Distribution for the Proposed Filters

For further validation by using the CST software simulator, Fig. 23 elaborates the current distribution of the reported pass band filters at the resonant frequencies.

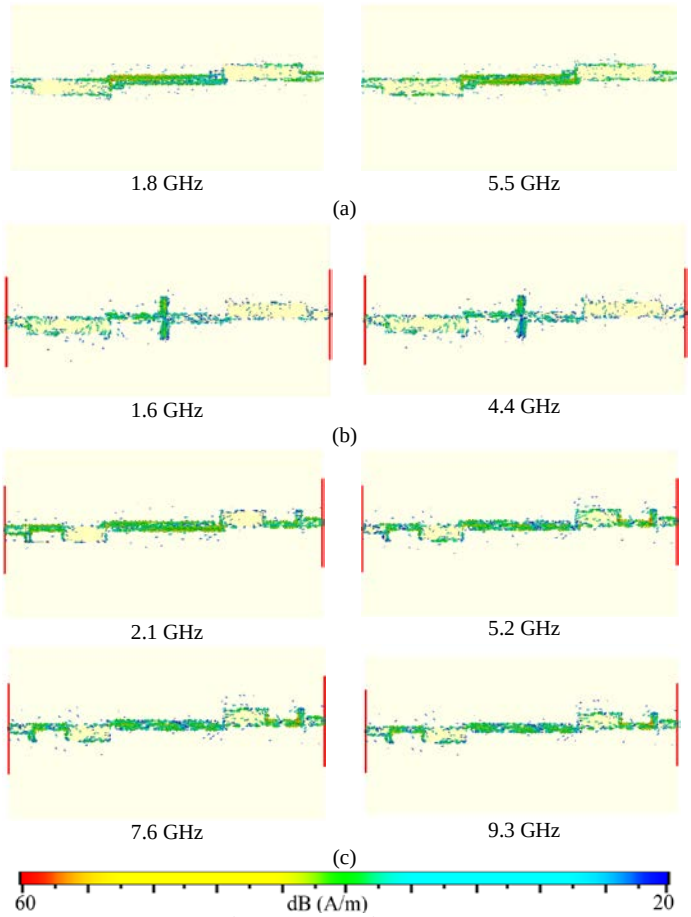

Fig. 23. Current distribution for the designed filters. (a) SS-ASIRs with ICCLs. (b) SS-ASIRs with PUMLs. (c) SS-ASIRs with DMS.

As shown in Fig. 23(a), the electric field is mainly distributed near the interdigital cross-coupled lines, with maximum current density 60 and 58 A/m at 1.8 and 5.5 GHz, respectively. But for Fig. 23(b), the electric field is mainly distributed near the parallel uncoupled microstrip lines, with maximum current densities 58 and 57 A/m at 1.6 and 4.4 GHz, respectively. On the other hand, as seen from Fig. 23(c), most of the currents are around the defected rectangular structures and the two coupled transmission lines with maximum current densities 60 A/m at 2.1, 5.2, 7.6 and 9.3 GHz. It is significant that the proposed designs can be easily developed to handle and permit reconfigurability [24] and can be easily integrated with antenna designs [25], to create the so-called "filtenna" [26].

IV. CONCLUSION

Multi-standard dual-wideband and quad-wideband filters based on the detailed analysis of the simple asymmetric stepped-impedance resonator unit and of the skew-symmetrical asymmetric stepped-impedance resonator coupled pair have been presented. By utilizing a novel modified skew-symmetrical asymmetric stepped-impedance resonator coupled pair with interdigital cross-coupled lines and parallel uncoupled microstrip lines, the dual-band filters for the first time among recently proposed dual-wideband filters realize dual-wideband with wide stop band restrictions. Their bandwidths are controllable by tuning relative parameters. By introducing a defected microstrip structure, a frequency band nearby the third spurious frequency is formed, resulting in a quad-wideband filter. The proposed dual-wideband and quad-wideband modified skew-symmetrical asymmetric stepped-impedance resonator filters cover communication applications including Global Positioning System, Global System For Mobile Communication, The Universal Mobile Telecommunications System, industrial, scientific and medical band, and IEEE 802.11 a/b/g/n/ac. The filters' measured results agree well with simulated results and theoretical predictions. The good in-band and out-of-band performance, compact size and simple structure make the proposed filters very promising for applications in future multi-standard wireless communication.

ACKNOWLEDGMENTS

This project has received funding from the European Union's Horizon 2020 research and innovation programme under grant agreement H2020-MSCA-ITN-2016 SECRET-722424.

REFERENCES

[1] H.W. Liu; B.P Ren; S. Li; X.H. Guan; P. Wen; X. Xiao and Y. Peng, "High-Temperature Superconducting Bandpass Filter Using Asymmetric Stepped-Impedance Resonators With Wide-Stopband Performance," *IEEE Trans. Applied Superconductivity*, vol.25, no.5, pp.1-6, Oct. 2015.

[2] Y.X. Tu, X.R. Guo, C.H. Wang and J.Jin, "An improved 860–960MHz fully integrated CMOS power amplifier designation for UHF RFID transmitter," *International Journal of Electronics and Communications*,vol.67, no.7,pp.574-577,2013.

[3] Y. C. Chang, C. H. Kao, M. H. Weng, and R. Y. Yang, "Design of the compact dual-band bandpass filter with high isolation for GPS/WLAN applications," *IEEE Microw. Wireless Compon. Lett*., vol. 19, no. 12, pp. 780-782, Dec. 2009.

[4] C. H. Kim and K. Chang, "Independently controllable dual-band bandpass filters using asymmetric stepped-impedance resonators," *IEEE Trans.Microw. Theory Techn*., vol. 59, no. 12, pp. 3037-3047, Dec. 2011.

[5] H. W. Wu and R. Y. Yang, "A new quad-band bandpass filter using asymmetric stepped impedance resonators," *IEEE Microw. Wireless Compon. Lett*., vol. 21, no. 4, pp. 203-205, Apr. 2011.

[6] C. H. Kim and K. Chang, "Wide-stopband bandpass filters using asymmetric stepped-impedance resonators," *IEEE Microw. Wireless Compon. Lett*., vol. 23, no. 2, pp. 69-71, Feb. 2013.

[7] Y. C. Chang, C. H. Kao, M. H. Weng, and R. Y. Yang, "Design of the compact wideband bandpass filter with low loss, high selectivity and wide stopband," *IEEE Microw. Wireless Compon. Lett.*, vol. 18, no. 12, pp. 770-772, Dec. 2008.

[8] Y.C. Li; H. Wong; Q. Xue, "Dual-Mode Dual-Band Bandpass Filter Based on a Stub-Loaded Patch Resonator," *IEEE Microw. Wireless Compon. Lett*., vol.21, no.10, pp.525-527, Oct. 2011.

[9] R. Q. Zhang; L.Zhu; Sha Luo, "Dual-Mode Dual-Band Bandpass Filter Using a Single Slotted Circular Patch Resonator," *IEEE Microw. Wireless Compon. Lett*., vol.22, no.5, pp.233-235, May.2012.

[10] R. Q. Zhang; Lei Zhu, "Synthesis and Design of Wideband Dual-Band Bandpass Filters With Controllable In-Band Ripple Factor and Dual-Band Isolation," *IEEE Trans. Microw. Theory Techn*., vol.61, no.5, pp.1820-1828, May 2013.

[11] J. Xu; W. Wu; C. Miao, "Compact Microstrip Dual-/Tri-/Quad-Band Bandpass Filter Using Open Stubs Loaded Shorted Stepped-Impedance Resonator," *IEEE Trans. Microw. Theory Techn*., vol.61, no.9, pp.3187-3199, Sept. 2013.

[12] R.Q. Zhang; L. Zhu, "Synthesis of Dual-Wideband Bandpass Filters With Source-Load Coupling Network," *IEEE Trans. Microw. Theory Techn*., vol.62, no.3, pp.441-449, March 2014.

[13] J. Li; S.S Huang; J.Z. Zhao, "Compact Dual-Wideband Bandpass Filter Using a Novel Penta-Mode Resonator (PMR)," *IEEE Trans. Microw. Theory Techn*., vol.24, no.10, pp.668-670, Oct. 2014.

[14] Sanchez-Soriano, M.A.; Gomez-Garcia, R, "Sharp-Rejection Wide-Band Dual-Band Bandpass Planar Filters With Broadly-Separated Passbands," *IEEE Microw. Wireless Compon. Lett*., vol.25, no.2, pp.97-99, Feb. 2015.

[15] H.W. Liu; Pin Wen; X.M. Wang; Y. Wang; etc, "Dual-Band High-Temperature Superconducting Hairpin-Resonator Bandpass Filter Based on Two Pairs of Nondegenerate Modes," *IEEE Trans. Applied Superconductivity*., vol.25, no.3, pp.1-4, June 2015.

[16] A.L.C. Serrano, F. S. Correra, T.-P. Vuong, and P. Ferrari, "Synthesis methodology applied to a tunable patch filter with independent frequency and bandwidth control,"*IEEE Trans. Microw. Theory Techn.*, vol. 60, no.3, pp.484-493, Mar. 2012.

[17] J. S. Hong and M. J. Lancaster, *Microstrip Filter for RF/Microwave Applications*. New York: Wiley, 2001.

[18] Tu, Y.; Ali, A.; Elmegri, F.; Abousitta, M.; etc, "novel multi-standard dual-wide band polygon SLSIR filter," *2015 Internet Technologies and Applications (ITA)*, pp.434-438, 2015.

[19] J. Xu; Wen Wu; C. Miao, "Compact and Sharp Skirts Microstrip Dual-Mode Dual-Band Bandpass Filter Using a Single Quadruple-Mode Resonator (QMR)," *IEEE Trans. Microw. Theory Techn*., vol.61, no.3, pp.1104-1113, March.2013.

[20] G. L. Matthaei, L. Young, and E. M. T. Jones, *Microstrip Filters, Impedance-Matching Network, and Coupling Structures*. Norwood, MA: Artech House, 1980.

[21] Tengfei Yan; Xiao-Hong Tang; Junfeng Wang, "A Novel Quad-Band Bandpass Filter Using Short Stub Loaded E-Shaped Resonators," *IEEE Microw. Wireless Compon. Lett*., vol.25, no.8, pp.508-510, Aug. 2015.

[22] Al-Yasir, Y. I. A., Abd-Alhameed, R. A., Noras, J., Abdulkhaleq, A. and Ojaroudi Parchin, N.: 'Design of Very Compact Combline Band-Pass

Filter for 5G Applications', Loughborough Antennas & Propagation Conference, 2018, Loughborough, UK.

[23] CST Microwave Studio, http://www.cst.com.

[24] Yuceer, m.: 'A reconfigurable microwave combline filter', *IEEE Transactions on Circuits and Systems II, Express Briefs*, 2016, 63, (1), pp. 84–88.

[25] Al-Yasir, Y. I. A, Abdullah, A, Mohammed, H, Abd-Alhameed, R and Noras, J: 'Design of Frequency-reconfigurable Multiband Compact Antenna using two PIN diodes for WLAN/WiMAX Applications', *IET Microwaves, Antennas and Propagation*, 2017, 11, (8), pp. 1098-1105.

[26] Atallah, H., Abdul Rahman, A., Yoshitomi, K. and Pokhare, P.: 'Compact frequency reconfigurable filtennas using varactor loaded t-shaped and h-shaped resonators for cognitive radio applications', *IET Microwaves, Antennas and Propagation*, 2016, 10, (9), pp. 991–1001.